Supporting Information for

Highly Branched and Defect-Rich PdP Nanosheets for Ethanol Oxidation Electrocatalysis

Hao Lv,[1,2] Yuxiang Teng,[1] Yaru Wang,[1] Dongdong Xu,[1,*] and Ben Liu[1,2,*]

[1]Jiangsu Key Laboratory of New Power Batteries, Jiangsu Collaborative Innovation Center of Biomedical Functional Materials, School of Chemistry and Materials Science, Nanjing Normal University, Nanjing 210023, China.

[2]College of Chemistry, Sichuan University, Chengdu 610064, China

*E-mails: ddxu@njnu.edu.cn (D. Xu); ben.liu@njnu.edu.cn (B. Liu)

Experimental Sections

Chemicals

Palladium (II) chloride ($PdCl_2$), L-ascorbic acid (AA), sodium hypophosphite (NaH_2PO_2), and commercial palladium carbon (Pd/C) were purchased from Alfa Aesar. Sodium hydroxide (NaOH), hydrochloric acid (HCl), and ethanol were obtained from Sinopharm Chemical Reagent Co. Ltd. Surfactant docosylpyridinium bromide was synthesized following the procedures in our previous report (*Chem. Sci., 2018, 9, 4451-4455*). H_2PdCl_4 solution (10 mM) was prepared by using $PdCl_2$, HCl solution, and deionized water. All above reagents were utilized without further purification with analytical reagent grade.

Synthesis of branched PdP NSs

In a typical synthesis, 17.0 mg of C_{22}-Py (Br^-) was first dissolved in 5.0 mL of deionized H_2O to obtain a homogeneous solution at 75 ^oC. After cooling down to room temperature, 0.15 mL of NaOH (100 mM), 0.2 mL of H_2PdCl_4 solution (10 mM) were added into the surfactant solution. The solution was moved into a water bath and further incubated at 50 ^oC for 30 min. Then, 0.5 mL of freshly prepared NaH_2PO_2 (0.034 M) was injected into above solution. After 12 h, PdP NSs were collected by centrifugation and washed several times with ethanol/H_2O. Pure branched Pd NSs were prepared by similar processes instead by using AA as the reducing agent. The proposed formation mechanism for PdP alloys was listed below (*Catal. Today 1998, 44, 3-16; Catal. Sci. Technol. 2016, 6, 6441-6447; Fuel Cells 2010, 3, 472-477*):

$$\mathbf{PdCl_4^{2-} + H_2PO_2^- + 2OH^- \rightarrow Pd + H_2PO_3^- + H_2O + 4Cl^-}$$
$$\mathbf{3H_2PO_2^- \rightarrow H_2PO_3^- + 2OH^- + H_2O + 2P}$$
$$\mathbf{H_2PO_2^- + H_2O \rightarrow H_2PO_3^- + H_2}$$
$$\mathbf{nPd + P \rightarrow Pd_nP}$$

Electrochemical ethanol oxidation

The electrocatalytic tests were performed on the CHI 660E electrochemical analyzer. A three-electrodes system was used for all electrochemical tests (a carbon rod as the counter electrode, a silver/silver chloride electrode (SCE) as the reference electrode, and PdP NSs coated onto glassy carbon electrode (GCE, 0.07065 cm^2) as the working electrode). A well-dispersed suspension of PdP catalyst was prepared by mixed solution of 1 mg nanocatalysts, 4 mg of Valcan XC-72, and 2 mL ethanol/ H_2O (1:3). After 25 μL of Nafion solution (5.0 wt %) was added and further treated under ultrasonic treatment for another 30 min. 6 μL above-prepared catalysts ink was coated onto pre-treated

GCE and dried before the electrocatalytic tests. Cyclic voltammograms (CVs) were scanned until the stabilized curves were obtained for further removal of the surfactant in 1.0 M KOH. CVs were employed to evaluate the ECSAs (1.0 M KOH) and activities (1.0 M KOH and 1.0 M ethanol) of the nanocatalysts at different scan rates.

Characterizations

Mesoscopic morphology and atomic crystallographic structure were characterized on a JEM-2100 transmission electron microscope (TEM) operated at 200 kV. Elemental mappings were collected on FEI Talos F200X apparatuses at an accelerating voltage of 200 kV (high-angle annular dark-field scanning TEM (HAADF-STEM)). Crystallographic structure was also studied with X-ray diffraction (XRD) on powder samples using a D/max 2500 VL/PC diffractometer (Japan) equipped with graphite-monochromatized Cu Kα radiation. Surface electronic states were performed on a scanning X-ray microprobe (Thermo ESCALAB 250Xi) under Al Kα radiation (X-ray photoelectron spectra (XPS)). Inductively coupled plasma mass spectrometry (ICP-MS) was tested on a NexION 350D.

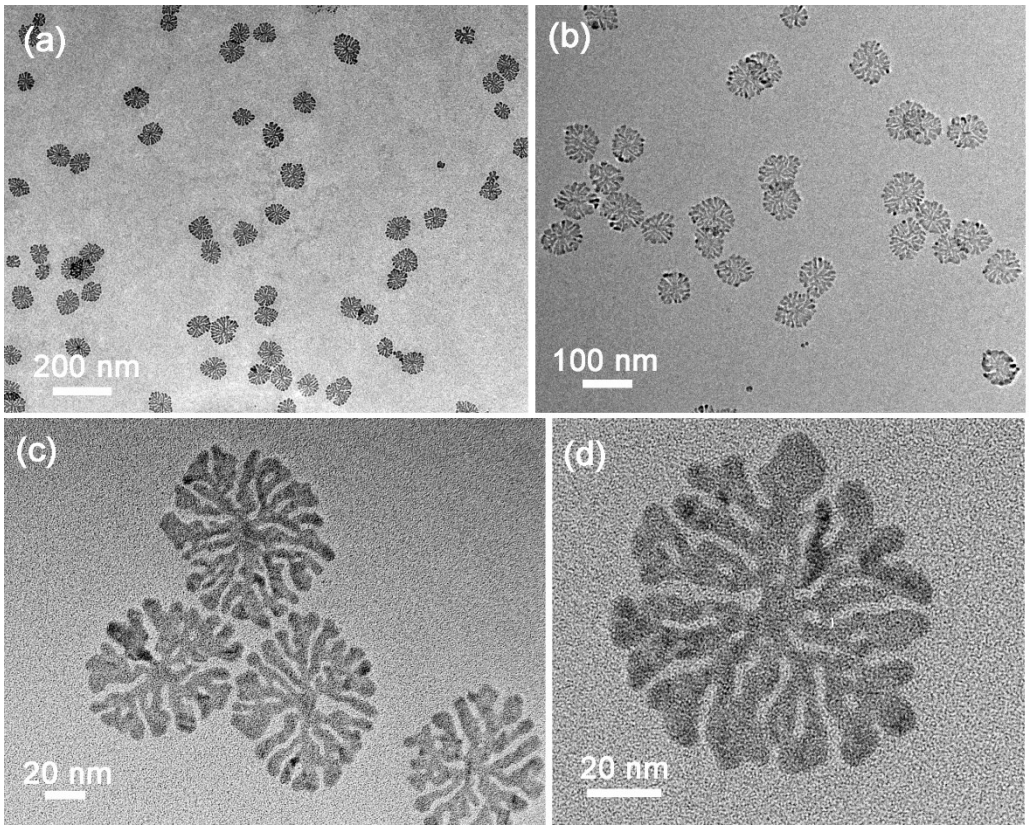

Fig. S1 (a-d) More TEM images of PdP NSs, confirming the generation of well-defined branched and ultrathin morphology.

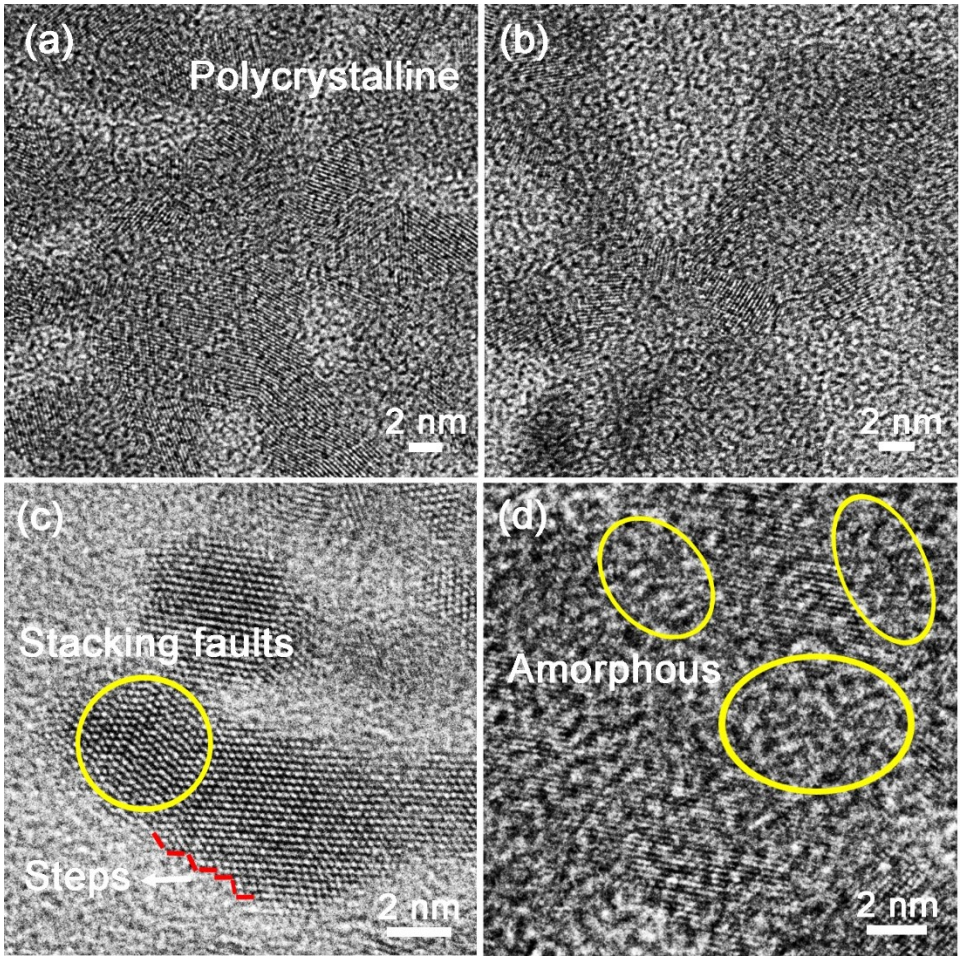

Fig. S2 (a-d) More HRTEM images of PdP NSs. There are abundant stacking faults, steps, amorphous domains inside PdP NSs, further confirming their defect-rich feature.

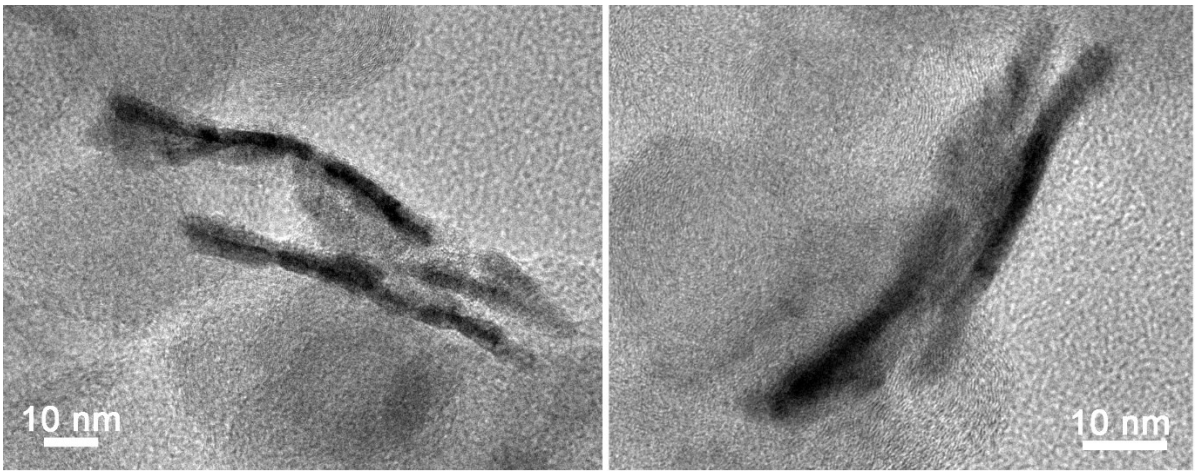

Fig. S3 More TEM images of PdP NSs, further confirming the ultrathin feature with the thickness of ~3.2 nm.

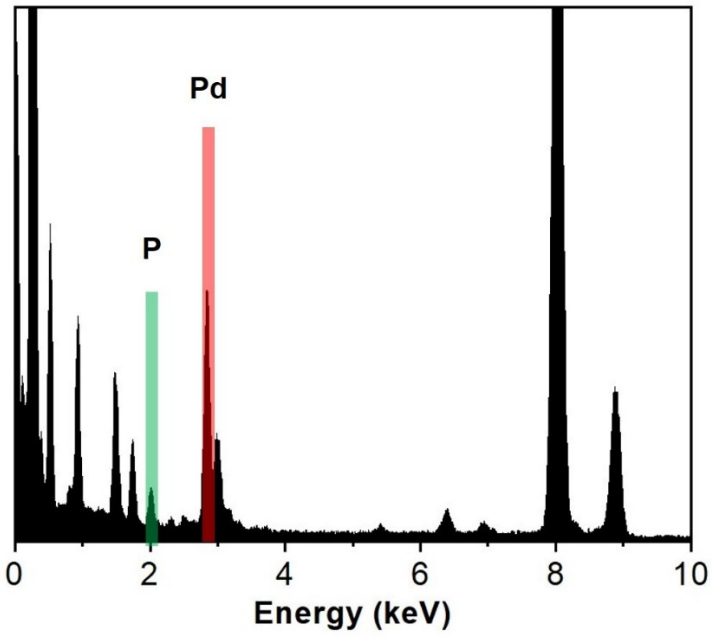

Fig. S4 EDS spectra of PdP NSs.

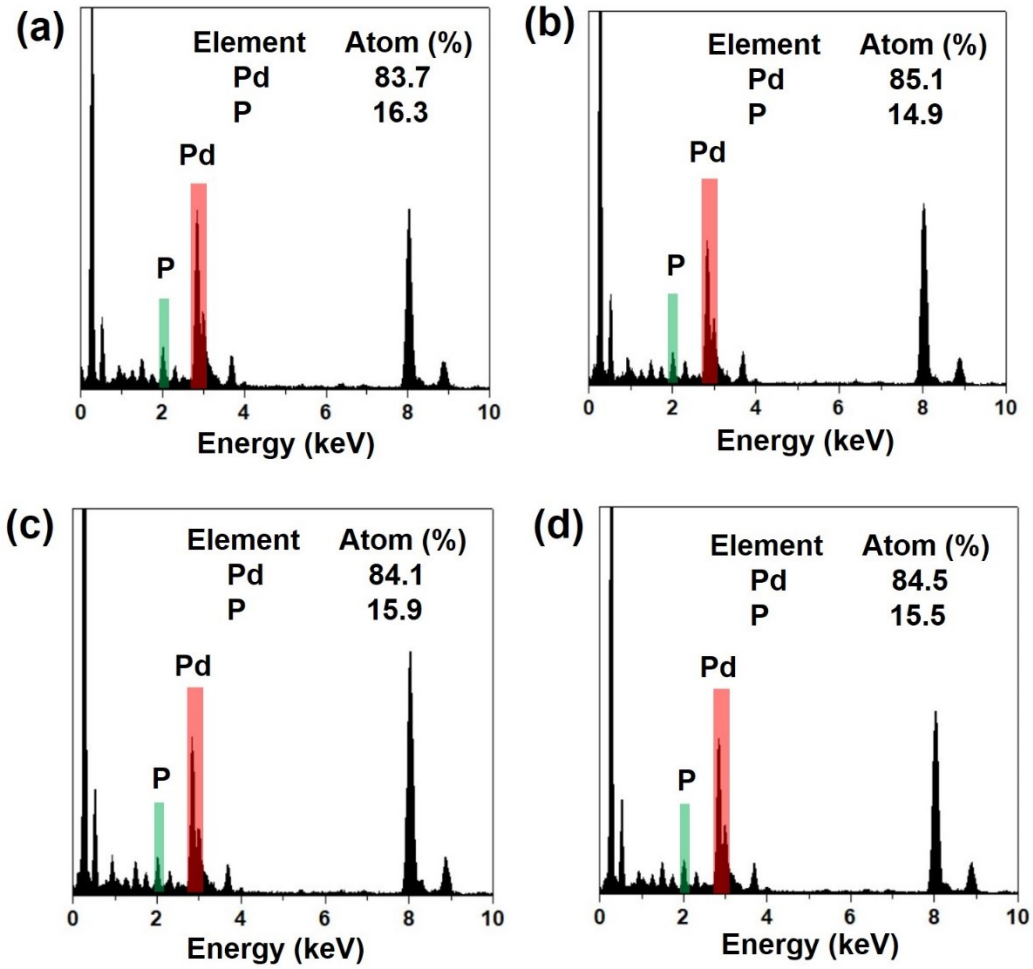

Fig. 5 (a-d) EDS spectra of PdP products obtained at the different crystalline growth period. The products correspond to the ones presented in Fig. 3a-d. The results indicated that the elemental ratio of Pd and P did not greatly change during the growth process.

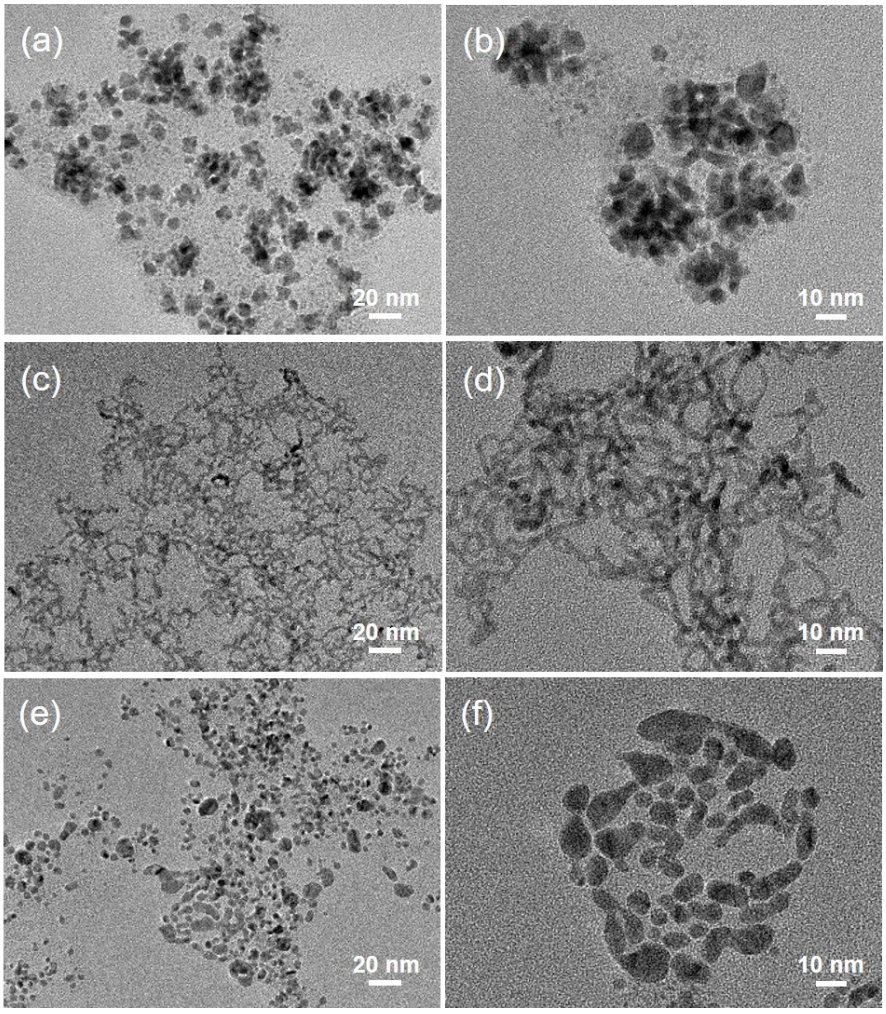

Fig. S6 TEM images of PdP crystals synthesized by different surfactants of (a-b) C_{16}-Py (Br^-), (c-d) DODAC, and (d-e) C_{22}-N (Br^-).

In the synthesis by surfactant cetylpyridinium bromide (C_{16}-Py (Br^-)) with a short hydrophobic carbon chain, branched PdP crystals but with larger thickness could be produced (Fig. S6a,b). Compared with the C_{22}-Py (Br^-) with a long carbon chain, C_{16}-Py (Br^-) missed the power to build stable lamellar micelles and further to confine the crystalline growth only along the in-plane orientation. Similarly, the surfactants, hexadecyl ammonium bromide (C_{22}-N (Br^-)) and dioctadecyldimethylammonium chloride (DODAC), were also unable to direct the construction of PdP nanosheets (Fig. S6c-f). Instead, only attached nanowires or nanoparticles were obtained. The weak nanoconfinement ability of these surfactants had been verified in our previous reports for the synthesis of monometallic Pd or Pt nanosheets. The synthesis results under different surfactants confirmed the crucial role of special surfactant as the nanoreactor for ultrathin PdP nanostructures.

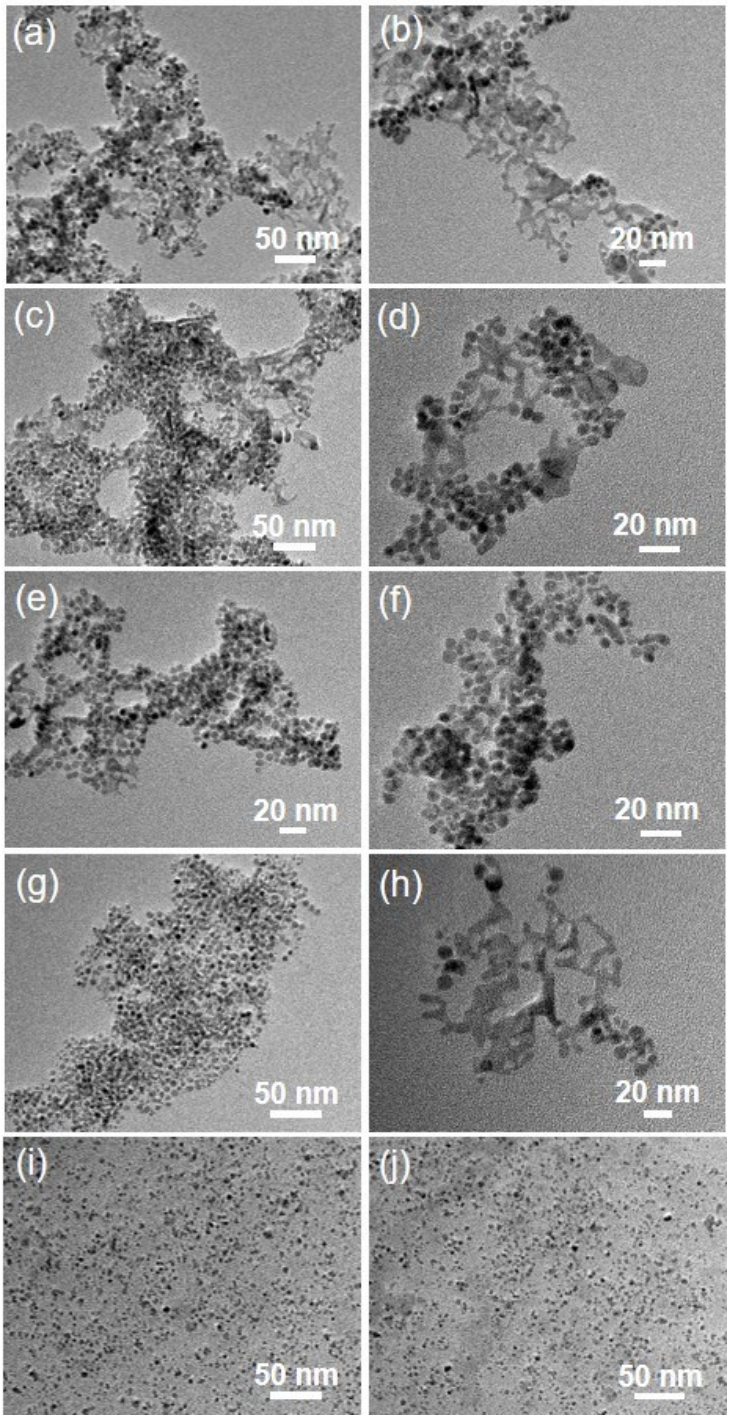

Fig. S7 TEM images of PdP crystals synthesized under different pH conditions of (a-b) 0.2 mL of 0.1 M HCl, (c-d) 0.05 mL of 0.1 M HCl, (e-f) without HCl or NaOH, (g-h) 0.05 mL of 0.1 M NaOH, and (i-j) 0.3 mL of 0.1 M NaOH. The other synthesis parameters kept the same with the synthesis of PdP NSs in this work.

The reduction rate of metallic precursor in elemental Pd or alloyed PdP by NaH_2PO_2 was greatly tailored *via* the change of pH value in the synthesis solution. Under acidic, neutral, and alkalescent

condition, NaH_2PO_2 possessed a relatively weak reduction ability and failed to produce enough initial PdP nanoplates for subsequent attachment growth. Instead, only thermodynamically stable nanoparticles or their networks were obtained under these pH conditions (Fig. S7a-h). However, the stronger alkaline environment also greatly modified the reduction kinetics, resulting in the generation of abundant small nanoparticles (Fig. S7i-j). Therefore, an optimum reduction and growth rate is necessary for the synthesis of ultrathin PdP NSs.

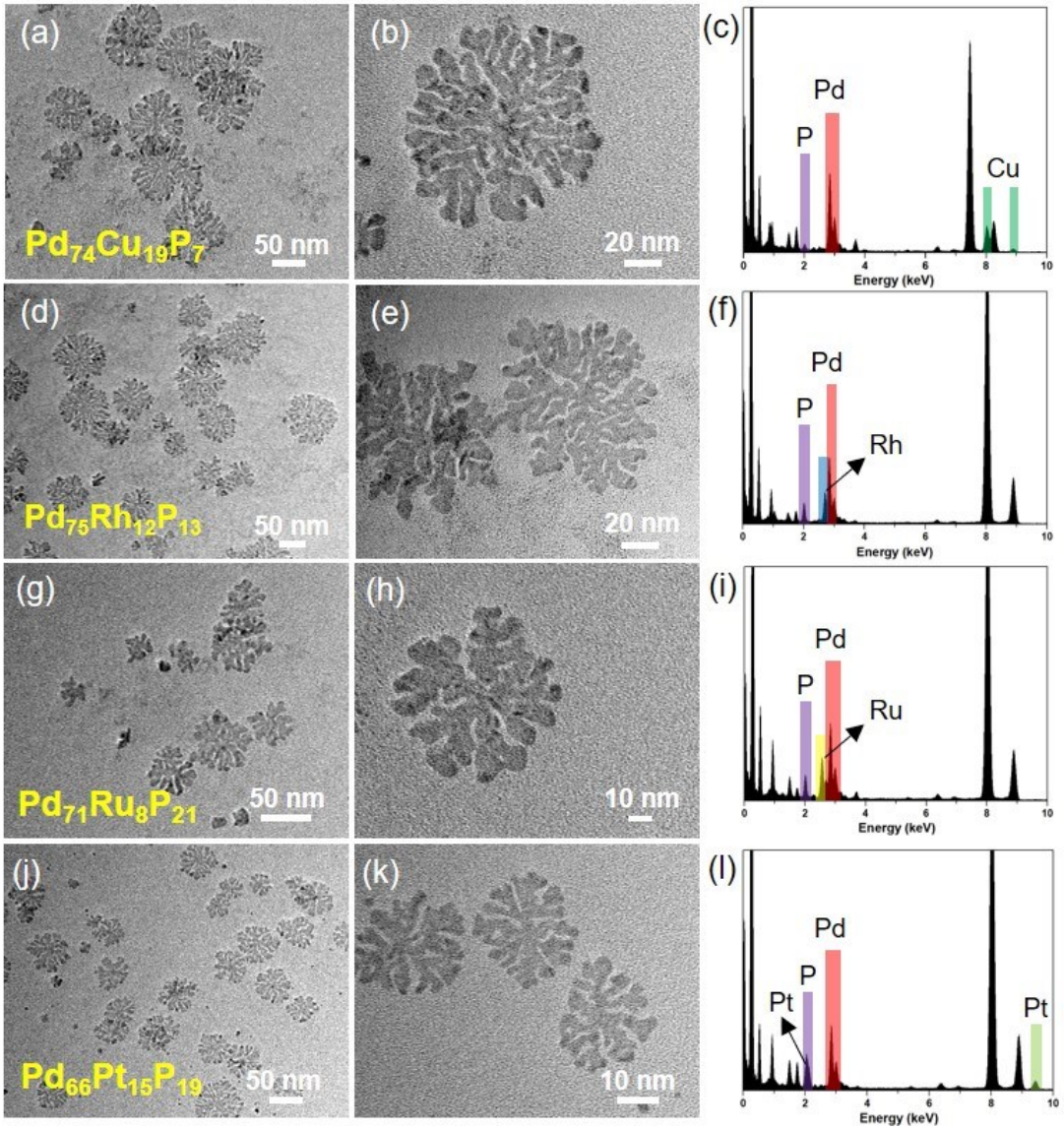

Fig. S8 (a, b, d, e, g, h, j, and k) TEM images and (c, f, i, and l) corresponding EDS spectra of ternary PdMP NSs, (a-c) PdCuP, (d-f) PdRhP, (g-i) PdRuP, and (j-l) PdPtP NSs.

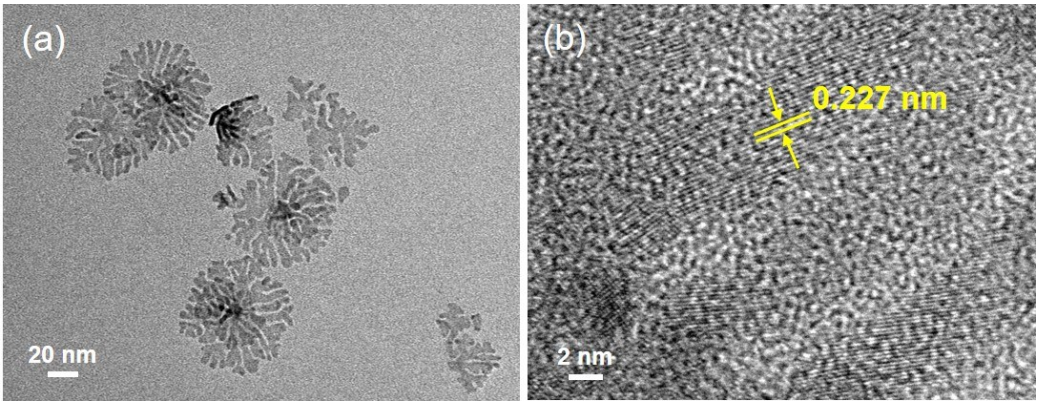

Fig. S9 (a) TEM and (b) HRTEM images of branched Pd nanosheets used as the comparison for EOR tests.

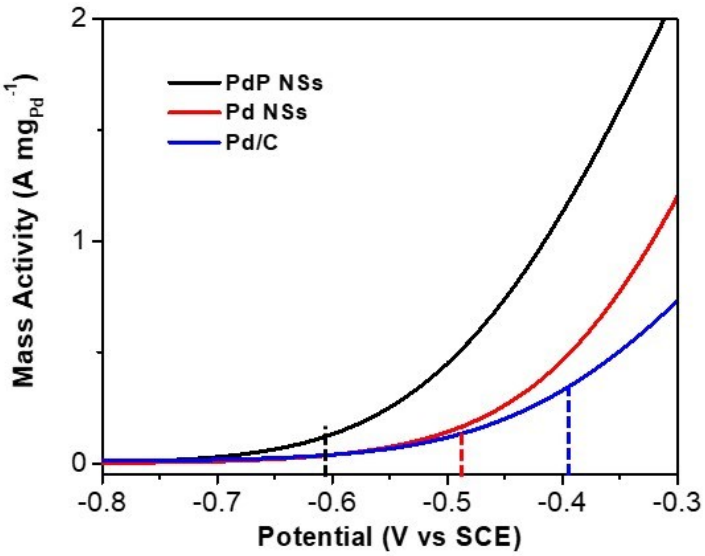

Fig. S10 Enlarged CV curves of PdP NSs, Pd NSs, and Pd/C in the potential range of -0.8 and -0.3 V.

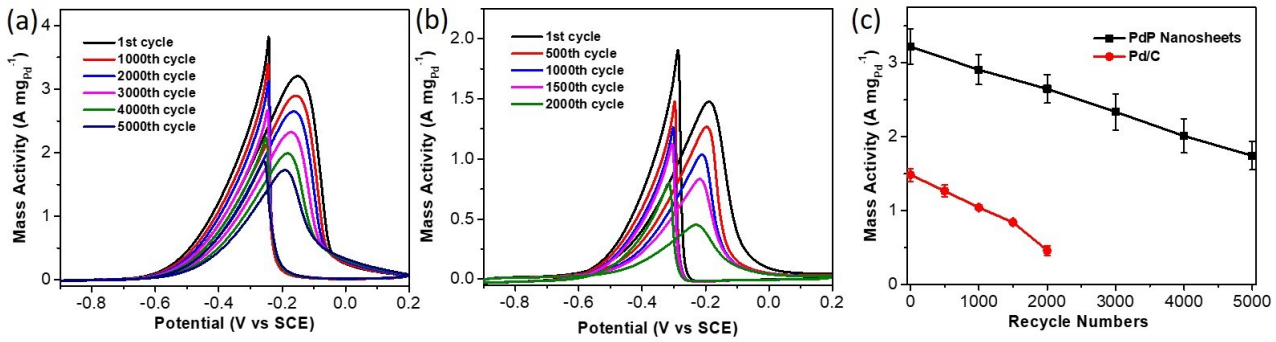

Fig. S11 CV curves of (a) PdP NSs and (b) Pd/C in the 1st, 1000th, 2000th, 3000th, 4000th, and 5000th in 1.0 M KOH and 1.0 M ethanol at a scan rate of 50 mV s^{-1}. (c) The tendency chart of mass activities versus cycle number.

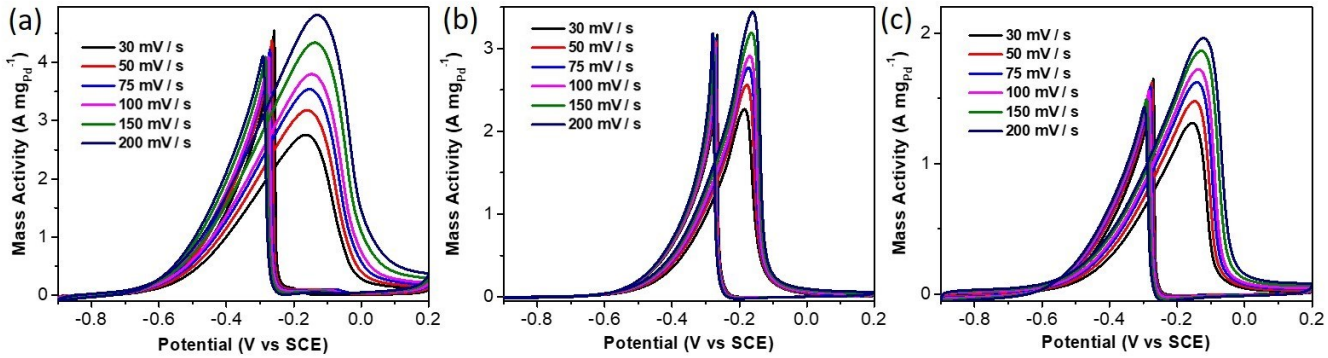

Fig. S12 CV curves of (a) PdP NSs, (b) Pd NSs, and (c) Pd/C with different scan rates (v) of 30-200 mV s^{-1} in 1.0 M KOH and 1.0 M ethanol.

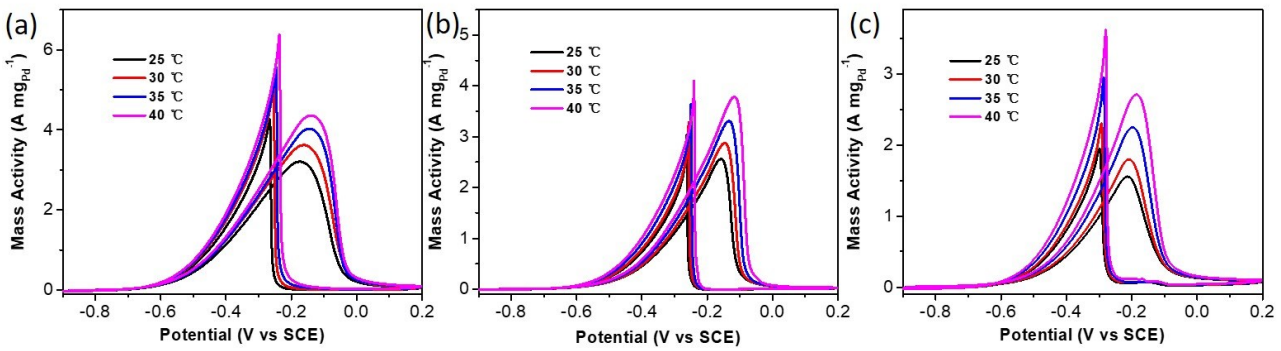

Fig. S13 CV curves of (a) PdP NSs, (b) Pd NSs, and (c) Pd/C under different temperatures of 25-40 ^{o}C in 1.0 M KOH and 1.0 M ethanol.

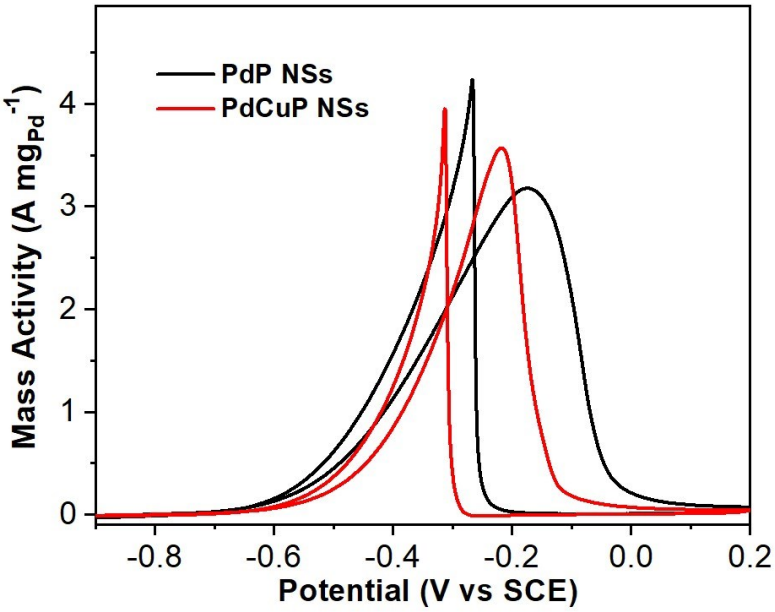

Fig. S14 CV curves of PdP and PdCuP NSs collected in 1.0 M KOH and 1.0 M ethanol, indicating enhanced mass activity of PdCuP NSs owing to the induction of another metal.

Electrocatalytic mechanism

The enhanced EOR performance of highly branched PdP NSs can be attributed to the synergistic effects of highly branched, ultrathin, defect-rich, and P-alloyed features. First, morphological nanosheets and nanodendrites provide more electrocatalytic active sites and higher atomic efficiency versus commercial Pd nanoparticles. In additional, the patulous framework in PdP NSs efficiently facilitates the mass/electron transfer during EOR. Second, rich crystallographic defects in PdP NSs, such as twins/nanotwins, stacking faults, grain boundaries, low-coordination number atoms (e.g.,

steps, corners, and edges), and amorphous arrangement, greatly boost the intrinsic electrocatalytic performance.[1] Third, when non-metal P atoms were alloyed into Pd nanocrystals, the electronic state of Pd can be greatly modified, resulting in weakening the adsorption or binding between Pd atoms and poisonous intermediates (e.g., CO_{ads} and CH_3CO_{ads}). On the other hand, sufficient OH_{ads} (P-OH_{ads}) formed owing to the presence of P atoms, which made the subsequent reaction with Pd-CH_3CO_{ads} (the rate-determining step in EOR) easier and faster. Synergistic compositional effect was also verified in the ternary PdCuP NSs (Fig. S14). Therefore, the electrocatalytic kinetics and electrocatalytic EOR performance of PdP NSs can be greatly accelerated.

Reference

1 (a) C. Li, Q. Yuan, B. Ni, T. He, S. Zhang, Y. Long, L. Gu, X. Wang, *Nat. Commun.,* **2018**, *9*, 3702; (b) Li, M., Duanmu, K., Wan, C. et al *Nat. Catal.,* 2019, *2*, 495; (c) H. Rong, J.,Mao, P. Xin, D. He, Y. Chen, D. Wang, Z. Niu, Y. Wu, Y. Li, Adv. Mater., 2016, 28, 2540.